Impacts of fully coupling land surface and flood models on large wetland's water dynamics: the case of the Inner Niger Delta

Augusto Getirana*[1,2], Sujay Kumar[1], Goutam Konapala[1,3], Christopher E. Ndehedehe[4]

[1]Hydrological Sciences Laboratory, NASA Goddard Space Flight Center, Greenbelt, MD, United States

[2] Science Applications International Corporation, Greenbelt, MD, United States

[3]Universities Space Research Association

[4]Australian Rivers Institute and Griffith School of Environment & Science, Griffith University, Nathan, Brisbane, Australia

*Corresponding author (augusto.getirana@nasa.gov)

Abstract

It is known that representing wetland dynamics in land surface modeling improves models' capacity to reproduce fluxes and land surface boundary conditions for atmospheric modeling in general circulation models. This study presents the development of the full coupling between the Noah-MP land surface model (LSM) and the HyMAP flood model in the NASA Land Information System and its application over the Inner Niger Delta (IND), a well-known hot-spot of strong land surface-atmosphere interactions in West Africa. Here, we define two experiments at 0.02º spatial resolution over the 2002-2018 period to quantify the impacts of the proposed developments on IND dynamics. One represents the one-way approach for simulating land surface and flooding processes (1-WAY), i.e., Noah-MP neglects surface water availability, and the proposed two-way coupling (2-WAY), where Noah-MP takes surface water availability into account in the vertical water and energy balance. Results show that accounting for two-way interactions between Noah-MP and HyMAP over IND improves all selected hydrological variables. Compared to 1-WAY, evapotranspiration derived from 2-WAY over flooding zones doubles, increased by 0.8mm/day, resulting in an additional water loss rate of ~18,900km^3/year, ~40% drop of wetland extent during wet seasons and major improvement in water level variability at multiple locations. Significant soil moisture increase and surface temperature drop were also observed. Wetland outflows decreased by 35%, resulting in a substantial a Nash-Sutcliffe coefficient improvement, from -0.73 to 0.79. It is anticipated that future developments in global water monitoring and water-related disaster warning systems will considerably benefit from these findings.

Key Points

1. The full coupling of land surface and flood models in NASA's Land Information System is described and evaluated over the Inner Niger Delta
2. Increased evapotranspiration resulted in an 18900km3/year water loss to the atmosphere, decreasing wetland outflows by 35% and extent by 40%
3. Compared to an uncoupled system, the proposed implementation resulted in substantial improvements of all selected hydrological variables

1. Introduction

In the past several years, the scientific community has witnessed an increasing availability of land data assimilation system (LDAS) products. Such systems are conceived to provide the community with spatially and temporally distributed water and energy states and fluxes at varying domains and scales. Some of them are the Global LDAS (GLDAS; Rodell et al., 2004), the North America LDAS (NLDAS; Xia et al., 2012), the Famine Early Warning System Network (FEWS NET) LDAS (FLDAS; (McNally et al., 2017) and the NASA Hydrological Forecast and Analysis System (NHyFAS; Arsenault et al., 2020). Many of them are built based on the NASA Land Information System (LIS) framework (Kumar et al., 2006) and take advantage of a wide range of models, datasets and assimilation schemes available in LIS. The suite of land surface models (LSMs) available in LIS compute the vertical water and energy balance and are coupled with the Hydrological Modeling and Analysis Platform (HyMAP) global scale river routing scheme (Getirana et al., 2012), which simulates the horizontal water dynamics on the land surface. The current modeling structure is performed as a one-way coupled system, meaning that, at each modeling time step, HyMAP is informed with spatially distributed LSM-based surface runoff and baseflow, which are routed through a prescribed river network, but does not provide any feedback to the LSM. In other words, LSMs are not informed on the spatial and temporal surface water availability (e.g., rivers, floodplains, wetlands, lakes and reservoirs), which could impact the vertical water and energy balances. The numerical representation of such bidirectional interactions between the land surface and surface waters is called hereafter two-way coupled system. The misrepresentation or absence of such a physical process in LSMs ultimately impacts water content in the different soil layers and its availability for plant transpiration, as well as bare soil and open water evaporation. Such impacts on evapotranspiration (ET) may result in misrepresented atmospheric fluxes, in particular within coupled land-atmosphere coupled systems, as commonly found Earth system models.

A few exceptions aside (e.g., Dadson et al., 2010; Decharme et al., 2012; Miguez-Macho et al., 2007), large-scale river routing and flood modeling is usually one-way coupled and oftentimes performed as a land surface modeling post-processing step (e.g., Getirana et al., 2014; Lin et al., 2019; Luo et al., 2017; Yamazaki et al., 2014). Miguez-Macho et al. (2007) introduced a continental-scale coupled groundwater-surface water model using the Land-Ecosystem-Atmosphere Feedback (LEAF2) LSM (Walko et al., 2000) and applied it over the U.S. at 12.5-km

spatial resolution. Among their findings, the authors showed how shallow water tables control river flow in specific locations. However, neglecting floodplains and using a simple linear reservoir model to represent river flow were limiting assumptions in order to accurately demonstrate the impacts of surface waters on the water budget. These limitations were addressed in a subsequent study (Miguez-Macho and Fan, 2012a), where the authors proposed the integration of a floodplain module and the use of a local inertia formulation (Bates et al., 2010) to represent surface water dynamics over the Amazon basin at a 2-km spatial resolution. Their simulations show two-way exchanges between surface waters and groundwater as infiltration in the wet season and seepage in the dry season. Dadson et al. (2010) evaluated the impacts of two-way coupling the Joint UK Land-Environment Simulator (JULES) LSM (Cox et al., 1999) with a linear reservoir model to represent rivers and floodplains within 0.5º grid cells over the upper Niger River, including its inner delta. A similar development was proposed by Decharme et al. (2012), where the Interaction Sol-Biosphere-Atmosphere (ISBA) LSM (Noilhan and Planton, 1989) is two-way coupled with a kinematic-wave-based river routing scheme that also represents floodplain water storage within grid cells. Kinematic wave is a simplified version of the one-dimensional Saint-Venant equations that is better suited for steep bed slopes and shallow flow, since it neglects downstream boundary condition. The study by Decharme et al. (2012) focused on analyzing the sensitivity of river geometry and floodplain parameters on representing global streamflow, flooded areas and evapotranspiration at 1º spatial resolution. In a follow-up study at the global scale Decharme et al. (2019) described an improved modeling system at 0.5º spatial resolution and reported an expected overall drop in global flooded extents and increase in soil moisture due to increased evaporation from open waters. On the other hand, the authors highlight that the modeling system simulates inundations only in grid cells that correspond to major streams, while, in reality, inundations also occur in areas adjacent to major streams. Such a limitation may underestimate the actual surface water impacts on other hydrological processes, particularly over large and dynamic water bodies. This means that finer resolutions are more appropriate when implementing two-way coupled modeling systems. More recently, using the Organizing Carbon and Hydrology In Dynamic Ecosystems (ORCHIDEE) LSM (Krinner et al., 2005) at 0.5º, Schrapffer et al. (2020) articulate the importance of representing large tropical floodplains in Pantanal in two-way coupled model simulations to improve their capacity in reproducing fluxes and land surface conditions. At a finer scale, Chaney et al. (2020) described a two-way coupling implementation at ~1km spatial

resolution, accounting for sub-grid information through hydrological response units. The vertical water and energy balances are computed using the Noah LSM with Multiparameterization options (Noah-MP; Niu et al., 2011) and the horizontal water redistribution through the kinematic wave equation.

Based on these recent efforts on two-way coupling developments, one can conclude that an accurate representation of surface water dynamics, in particular wetlands and floodplains, is essential to reproduce the surface water impacts on the land surface and the atmosphere. At coarse spatial resolutions, some large water bodies can be represented by a single grid cell. However, as resolutions get finer with model developments, better interactions between grids are needed in order to represent wetlands and floodplains. Hence, the use of advanced river and floodplain dynamic formulations in large-scale river routing schemes are essential (Getirana et al., 2017a; Luo et al., 2017; Miguez-Macho and Fan, 2012a; Yamazaki et al., 2014). Taking advantage of a local inertia implementation combined with a reservoir operation scheme, Getirana et al. (2020b) demonstrated the potential of HyMAP in simulating reservoir operation impacts on Lake Victoria's outflow and surface water extent, storage and elevation. The authors argue that, despite the overall good agreement with observations, the fact that HyMAP was one-way coupled with Noah-MP may have resulted in a misrepresentation of evapotranspiration and infiltration over the lake.

Motivated by previously mentioned needs for an integrated modeling system to more accurately represent physical processes in land surface models, in particular over wetlands, this study presents the two-way coupling between HyMAP and Noah-MP models in LIS and quantify its impacts on key hydrological processes. As discussed above, the increasing need for multi-model LDAS frameworks require two-way coupled systems that can be flexible to implement with multiple models. On the other hand, current two-way coupled systems are typically composed of single pairs of LSMs and river routing schemes, tailored to specific Earth system models. A key contribution of this article, therefore, is the description of a generalized implementation of two-way coupling using the range of LSMs integrated in LIS, paving the potential use within integrated Earth system models.

The Inner Niger Delta (IND) region is selected as the study area for being a large wetland located in the West African semi-arid climate zone, where surface water feedback to the soil and the

atmosphere plays a major role in the vertical water and energy balances. The IND region is a key water tower in West Africa and is susceptible to the impacts of climate change. Rainfall and hydrological sinks such as evapotranspiration are crucial to changes in stored water, especially in IND where deforestation is high (James et al., 2007) and could impact on atmospheric moisture. While precipitation in the IND is an important driver of surface water hydrology and terrestrial stored water in general (Ndehedehe et al., 2016), its nature and characteristics could be complex. Changes in atmospheric circulation patterns induce variations in circulation between source and sink terms, thus redirecting moisture (Gimeno et al., 2010). This, in turn, leads to considerable changes in water stored in wetlands, reservoirs as well as floodplains in these areas (Ndehedehe et al., 2016). For this region, global reanalysis observations and land surface models that provide atmospheric fields, and water fluxes can therefore be improved by including their interactions with floodplains dynamics.

The scientific goal of this study is to improve our current understanding of how two-way coupling LSMs and river routing schemes impacts the representation of hydrological processes over large wetlands, focusing on the IND domain. We attempt to use the most appropriately known meteorological forcings and parameters available for the region and assume that the resulting modeling system is the best possible representation of hydrological processes over the wetland. We understand and acknowledge all limitations intrinsic to numerically representing physical processes with the proposed models, which include assumptions, simplifications and inaccuracy in both parameterizations and boundary conditions (e.g., meteorological forcings). Such limitations are accounted for in our discussions, but their assessment (including sensitivity tests) is beyond the scope of this study.

2. Datasets and methods

2.1. Datasets

Model experiments were evaluated with daily streamflow observations, satellite-based altimetry, water extent and evapotranspiration. Daily streamflow observations were made available at three gauging stations within or in the surroundings of the domain by the *Comité permanent Inter état de Lutte contre la Sécheresse au Sahel* (CILSS), as described in (Getirana et al., 2020a). Two of them are located upstream the wetland at Koulikoro and Pankourou, on the Niger and Bagoé

Rivers, respectively. These gauges are located around 330km and 400km upstream the wetland and drain areas of 120,000km^2 and 35,080km^2, respectively. Two other stations are located within the domain, one upstream the wetland at Ké Mecina, draining 137,150km^2, and another downstream at Diré, draining 362,280km^2. Table 1 provides additional information about these stations and Figure 1 shows locations of Ké Mecina and Diré gauging stations. These two gauging stations are ~470km apart from each other. Monthly streamflow climatologies at Ké Mecina and Diré (Figure 1) indicate a substantial diffusiveness caused by the wetland, resulting in a two-month lag and drop of flood peak magnitude. Koulikoro and Pankourou are used in our model to define upstream boundary conditions, as described below. Due to its proximity to the upstream limits and little influence by the wetland, Ké Mecina is only used here for illustrative purposes.

Radar altimetry time series are those made available on the Hydrosat database (Tourian et al., 2017). Hydrosat is composed of multi-satellite radar altimetry data following the approach described in Tourian et al. (2016) that produces ~3-day time step water level time series from the original sub-monthly or monthly datasets by hydraulically and statistically connecting nearby locations. Time series available over the Niger River are composed of measurements derived from the ENVISAT, Jason-2 and SARAL/AltiKa missions, with reported mean absolute errors over inland waters in the order of few decimeters, depending on the sensor, water body size and the crossing angle of the altimeter track (Calmant et al., 2013; O'Loughlin et al., 2016; Santos da Silva et al., 2010; Tourian et al., 2017; Yamazaki et al., 2017). Here, we used radar altimetry time series at four locations within the IND domain with data available from 2002 to 2015. Global lidar measurements derived from the Ice, Cloud, and land Elevation Satellite (ICESat) mission are available from 2003 to 2009 on the OpenAltimetry database (https://openaltimetry.org). Masks over eight ICESat track intersections with water bodies were manually defined and time series were automatically extracted from the database. An intersection is defined by all water body transects within a 2-km river reach. An average of four observations per water body transect were grouped based on the date of observation. This means that, at an intersection, the median of observations on the same day defines the water elevation at that date. As a result, time series at intersections are composed of 11-15 dates (or transects), varying as a function of the location. The mean absolute error of ICESat over inland waters is ~0.1m (O'Loughlin et al., 2016; Urban et al., 2008). Figure 1 shows locations where radar and lidar altimetry time series are available within

188 the IND domain, where radar altimetry locations are numbered from H1 to H4 and laser altimetry
189 locations from I1 to I8.

190 Monthly water extent maps of the Niger basin were generated for the 2002-2018 period by a trained
191 deep learning algorithm known as U-Net (Ronneberger et al., 2015). U-net is trained on 446 hand-
192 labeled chips with 250 meter resolution of eleven flood events across the globe as provided by
193 Sen1Floods11 Dataset (Bonafilia et al., 2020). The Sen1Floods11 was originally intended for
194 usage with Sentinel 1, but here, we resampled the hand-labeled water extent chips to a lower
195 resolution to match MODIS data spatial resolution. Eight-day MODIS data composites for all the
196 eleven flood events within a period of ten days of the flood event was downloaded for our task. U-
197 Net was trained with all the eight Terra MODIS bands as an input and the hand-labeled water
198 extent maps as output. The algorithm was trained to decrease the binary classification error by
199 incorporating F-Score as our loss function. F-score ranges from 1, indicating perfect overlap of
200 water and land pixels between predicted and observed pixels, to 0, indicating no overlap. The
201 algorithm achieved an average F-score of 0.9, 0.88 and 0.76 during the training phase, validating
202 and testing phase, respectively. Our trained U-Net was used to generate water extent maps for the
203 IND domain with eight-day MODIS imagery from 2002 to 2018. Maps were aggregated to the
204 monthly time step. Figure 1 shows an occurrence map.

205 The impact of the two-way coupling on modeled evapotranspiration fields was evaluated using
206 three reference datasets. One is the 10-km, monthly FLUXCOM product (M. Jung et al., 2019),
207 developed from merging energy flux measurements from eddy covariance towers with MODIS
208 data, and available during 2001-2015. Another reference ET estimate is the 0.25°, daily Global
209 Land Evaporation Amsterdam Model (GLEAM) version 3.3a (Martens et al., 2017) data, a
210 primarily passive microwave remote sensing–based, Priestley Taylor evaporation model product
211 available during 1980–2018. We also used the 4-km, daily Atmosphere–Land Exchange Inverse
212 (ALEXI; Anderson et al., 2007), a MODIS-thermal-infrared based evapotranspiration product
213 available during 2001–present (Hain and Anderson, 2017). Although all these products integrate
214 various sources with different methodologies and have random and bias errors of their own, they
215 all use MODIS data in their algorithms. In this sense, they will be referred hereafter as satellite-
216 based ET estimates.

217 **2.2.Modeling framework**

HyMAP

HyMAP is a state-of-the-art global scale hydrodynamic model capable of simulating surface water dynamics, including water storage, elevation and discharge in-stream, as well as in floodplains. HyMAP simulates water dynamics in rivers and floodplains using the local inertia formulation (Bates et al., 2010; De Almeida et al., 2012; Getirana et al., 2017b), solving the full momentum equation of open channel flow and accounting for a more stable and computationally efficient representation of river flow diffusiveness and inertia of large water mass of deep flow, which is essential for a physically-based representation of wetlands, floodplains, tidal effects and impoundments (Getirana et al., 2020b). The Courant–Freidrichs–Levy (CFL) condition is used to determine HyMAP's optimal sub time steps for numerical stability. Rivers and floodplains interact laterally and have independent flow dynamics, with roughness and geometry derived from land cover characteristics, topography and river parameterization (Getirana et al., 2013, 2012). Hypsographic curves, i.e., the relationship between water elevation (H) and storage (S) are derived from high resolution topographic data. In addition to S, the flooded area (A) within a grid cell can also be determined through a relationship with H. As a result, floodplain water extent and storage can be derived from the floodplain water elevation with H×S×A relationships. If the water volume within a grid cell is above zero, the minimum A value corresponds to the river area (river length × river width) and it only increases once the river overflows to floodplains, with the grid area as the maximum value. The H×S×A relationship is derived for each grid cell from a pre-processing step where high resolution topography is upscaled to the model spatial resolution. Water overflows to floodplains when the river channel water height is higher than the bank height. This process is considered instantaneous at each time step. This means that water surface elevations of the river channel and the floodplain are the same.

Digital elevation model (DEM) accuracy plays an essential role in representing river network and floodplain extent in flat areas (Getirana et al., 2009a, 2009b). In this study, HyMAP parameters were derived from the Multi-Error-Removed Improved-Terrain (MERIT; Yamazaki et al., 2017) DEM at 3-arcsec spatial resolution. Over the IND domain, MERIT DEM is based on the NASA Shuttle Radar Topography Mission (SRTM; Farr et al., 2007) processed with successive correction of absolute bias, stripe noise, speckle noise, and tree height bias from using multiple satellite data sets and filtering techniques. As a result, MERIT DEM provides a more reliable representation of floodplains and wetlands than the original RSTM DEM.

River geometry is represented by rectangular cross sections and large width-to-depth ratio. Widths of major rivers were derived from the MERIT-Hydro dataset (Yamazaki et al., 2019). MERIT-Hydro provides 90-m global river width estimates derived from Landsat data. River width of smaller tributaries not detected by the dataset were derived from the following empirical equation

$$w = max\left(0.2, 20 \times Q_{med}^{0.5}\right) \quad (1)$$

where w [m] is the average river width within a grid cell and Q_{med} [m^3/s] the annual mean discharge estimated using the global runoff ensemble from Getirana et al. (2014).

River width and bankfull height, h [m], was estimated using the following empirical equation:

$$h = max(0.35, \alpha \times w) \qquad \alpha = 2.6 \times 10^{-3} \quad (2)$$

Both equations (1) and (2) are derived from Getirana et al. (2012) and adapted for a finer spatial resolution. River channel roughness coefficients vary as a function of h, (for example, values are ~0.03 and ~0.04 over the Niger and Benue Rivers, respectively; roughness increases to 0.07 over the smallest tributaries). The Manning coefficient for floodplains is spatially distributed as a function of vegetation types derived from a static map (Masson et al. 2003), where larger values correspond to dense vegetated areas and lower values to sparser vegetated regions. Floodplain roughness varies from 0.035 to 0.075 within the domain. More details on HyMAP parameterization can be found in Getirana et al. (2012).

HyMAP resolves the local inertia formulation unidimensionally (i.e., an unique flow direction is attributed to each grid cell) and does not currently represent bifurcations, which is particularly important over deltas and flat areas (Yamazaki et al., 2014). However, its capability of simulating backwater effects combined and interactions between rivers and floodplains results in a pseudo two-dimensional representation of surface water dynamics. HyMAP has been extensively evaluated in the Amazon basin (Getirana et al., 2013; Getirana and Peters-Lidard, 2013) and adopted as a tool for regional (Getirana et al., 2014; Jung et al., 2017; Kumar et al., 2015a, 2016) and global (Getirana et al., 2017a) water cycle studies.

Noah-MP

The Noah with Multi-Parameterization (Noah-MP; Niu et al., 2011; Yang et al., 2011) LSM is used to simulate the vertical water and energy balances over the city. The Noah-MP LSM builds upon the well-known Noah LSM (Ek et al., 2003), which has been used in a variety of operational

models, applications and research studies. Noah-MP contains four soil layers totaling two meters down the land surface and different parameterization and physics options, which include different static vegetation and dynamic vegetation schemes, canopy resistance effects, radiation transfer (e.g., two-stream approximation), runoff and groundwater schemes, snow model options, and even crop and urban canopy schemes. We apply the prescribed vegetation scheme, based on monthly leaf area index climatology. The TOPMODEL simulated groundwater scheme (Niu et al., 2007) is selected, and the Noah-based lower boundary of soil temperature option is applied. Other climatology-based vegetation and albedo parameter maps include monthly greenness fraction (Csiszar and Gutman, 1999) and global (snow-free) albedo (Csiszar and Gutman, 1999). Table 2 summarizes the main schemes used in Noah-MP.

Model coupling

As noted earlier, the interactions between the LSMs in LIS and HyMAP are enabled in a generic manner using the standardized software tools and paradigms enabled by the Earth System Modeling Framework (ESMF; Hill et al., 2004). ESMF is a framework for building coupled Earth system models in an interoperable manner. For enabling coupled interactions between components, ESMF provides generic data structures to store and represent data that are being exchanged. We employ these capabilities to develop a flexible interface between HyMAP and LSMs for both one and two-way coupling, as shown in Figure 2.

In the one-way coupling mode, at the end of each LSM time step t, surface runoff and baseflow rates are transferred from the LSM to HyMAP. The LSM packages these fields as an ESMF object and "exports" them to HyMAP. Once these "import" states are received, HyMAP converts them into water volume as a function of HyMAP's time step t_h and grid cell size. That water volume is then summed to the surface water storage SWS [mm] at the end of t_h and propagated through the river reach on the following time step t_h+1. There is no feedback from HyMAP to the LSMs. In the two-way coupling mode, SWS and surface water extent computed at t-1 is divided time step period dt are created as the export state from HyMAP to the LSM. The LSM then employs it to update the soil surface states and fluxes in the following time step t. Over a non-saturated soil, that additional water may infiltrate, increasing soil moisture and, subsequently, evapotranspiration. The increased water availability in the soil also impacts the energy balance, resulting in a drop in

surface temperature. The remaining water flux is converted back to water volume and routed by HyMAP through the river network in the following time step t+1.

As the exchange states are defined using generic ESMF objects, this design allows the configuration of any LSM within LIS for use with HyMAP without significant model development efforts. The requirement for one-way coupling is that the LSM must define the surface runoff and baseflow fields. Similarly, if the LSM is to be used in a two-way coupled mode, the LSM must define the set of steps to update the soil states in response to the input surface water storage and extent information.

Experimental design

The modeling system was implemented for the domain defined by the coordinates 7.2°E – 2.2°E and 12.1°N – 17.1°N at a 0.02° spatial resolution. Two experiments were defined in order to quantify the impact of the proposed two-way coupling system on IND: one representing the traditional uncoupled approach for simulating land surface and flooding processes (called 1-WAY hereafter) and the proposed full land surface – flood coupling (called 2-WAY hereafter). Both modeling experiments were performed using upstream boundary conditions derived from a model run at 0.25° spatial resolution for the entire basin following the modeling protocol described in Getirana et al. (2020a) and in Appendix A.1. In order to optimize streamflow outputs from this coarser resolution run, available streamflow observations at Koulikoro and Pankourou gauging stations were directly inserted and propagated through the river network. Daily coarse resolution streamflow outputs were used as upstream boundary conditions in the proposed modeling experiments at two locations defined in Figure 1 as Niger inflow and Beni inflow. Constraining upstream boundary conditions is recommended in order to isolate errors in physical processes evaluated in this study.

Models were driven with NASA's Modern-Era Retrospective analysis for Research and Applications, version 2 (MERRA-2; Reichle et al., 2017) meteorological dataset, and precipitation from the Climate Hazards Group InfraRed Precipitation with Station data, version 2 (CHIRPS; Funk et al., 2015), which utilizes satellite-based estimates and station-based precipitation. CHIRPS station-based component contributes to a superior spatial and temporal precipitation distribution in the continent, as demonstrated by several studies (e.g., Bichet and Diedhiou, 2018; Dembélé and Zwart, 2016; Dinku et al., 2018; Poméon et al., 2017) and, as a result, it has been widely used

in monitoring water availability and forecast in Africa (Getirana et al., 2020a; Jung et al., 2017; McNally et al., 2019; Shukla et al., 2019). Model runs were first spun up for 60 years, allowing the models' water storage components to stabilize, followed by the 2002-2018 period experiments at a 15-minute time step. All model parameters, initial conditions and inputs were preprocessed using the Land surface Data Toolkit (LDT; Arsenault et al., 2018).

Evaluation procedure

The proposed wo-way coupled modeling system was quantitatively evaluated in terms of changes in key water flux (i.e., evapotranspiration and streamflow) and surface water storage proxy (i.e., water level and extent dynamics) variables over the IND wetland. Such changes were quantified through well-known metrics computed using *in situ* observations and satellite estimates described above as references. These metrics are the root mean square error (RMSE), Nash-Sutcliffe (NS) coefficient, bias, correlation (r) and variability ratio (γ) between simulation (s) and observation (o). RMSE, NS and γ are defined as follows:

$$\mathrm{RMSE} = \left[\frac{\sum_{t=1}^{nt}(s_t - o_t)^2}{nt}\right]^{1/2} \quad (3)$$

$$NS = 1 - \frac{\sum_{t=1}^{nt}(o_t - s_t)^2}{\sum_{t=1}^{nt}(o_t - \bar{o})^2} \quad (4)$$

$$\gamma = \frac{\sigma_s}{\sigma_o} \quad (5)$$

where t is the time step, nt the period length, $\bar{o}$ the mean value of the observations and σ the standard deviation. RMSE ranges from zero to ∞, where zero is the optimal case. NS ranges from –∞ to 1, where 1 is the optimal case, while zero means that simulations represent observed signals as well as the average of observations. γ ranges from zero to ∞, where 1 means that simulated and observed time series have identical variabilities. r ranges from -1 to 1, where 1 is the optimal case. The timing of simulated streamflow peaks was evaluated using the delay index (DI). DI is computed using the cross-correlation function R=f(m) between simulated and observed time series, where DI equals the value of the time lag m when R is maximized (Paiva et al., 2013b).

Following Kumar et al. (2014), we used selected evaluation metrics in the form of normalized information contribution (NIC) applied to the Nash-Sutcliffe (NS) coefficient, correlation (r), and the root mean square error (RMSE) between simulations (s) and observations (o). NIC applied to

these metrics is useful to determine the overall improvements resulting from 2-WAY compared to the 1-WAY run. Their respective NIC values are defined below:

$$NS_{NIC} = \frac{(NS_{2way} - NS_{1way})}{(1 - NS_{1way})} \quad (6)$$

$$RMSE_{NIC} = \frac{(RMSE_{1way} - RMSE_{2way})}{RMSE_{1way}} \quad (7)$$

$$r_{NIC} = \frac{(r_{2way} - r_{1way})}{(1 - r_{1way})} \quad (8)$$

All three metrics range from $-\infty$ to 1, where values above zero indicate improvement, below zero indicates degradation, and zero means no added skill. These three metrics were used in the evaluation of water level dynamics, in order to more easily summarize results at numerous locations.

Monthly surface water extent simulations were evaluated in terms of bias, correlation and variability ratio γ. Daily water level simulations were compared against observations at twelve locations where radar and lidar altimetry data are available using NIC metrics. Monthly evapotranspiration simulations were evaluated in terms of bias, correlation, γ and NS. Daily streamflow simulations were evaluated at the Diré gauging station using bias, DI, γ and NS coefficients. In addition to the quantitative analysis, spatially distributed surface water extent and evapotranspiration were qualitatively evaluated through visual inspection.

3. Results

3.1. Impacts on surface water dynamics

MODIS-based water extent over 2002-2018 averages 4690km^2, with peaks occurring between September and November and averaging ~11,150km^2 (Figure 3a). The highest monthly averaged water extents detected by MODIS were above 17,500km^2 and occurred in September 2010 and October 2018. The wetland generally dries out in April-June with an averaged water extent of 390km^2 (Figure 3d). By resolving surface water dynamics with the local inertia solution, diffusion and inertia in both rivers and floodplains are represented in model experiments. Simulations show the water redistribution over the wetland and nearby lakes. The 1-WAY experiment shows significantly overestimated water extent estimates, averaging 17,940km^2 during wet seasons

(Figure 3b), or 61% above MODIS estimates. Water extent simulated with 1-WAY over the study period is 14,800km^2,which represents a 215% overestimation compared to the MODIS estimates. Water extent is particularly highly overestimated during the dry seasons; 1-WAY averaged estimate in April-June is 11,460km^2, which is 29 times the extent detected by MODIS (Figure 3d). Wetlands derived from 1-WAY are concentrated in the central portion of the study domain. However, one can observe that part of it is located downstream the MODIS-based wetland, over an area dominated by intermittent lakes. As a result, wetlands are underestimated in the central portion of the domain and overestimated toward the northeast (Figure 3e). These differences can be explained by the numerous bifurcations that occur along the Niger River over IND flat areas, resulting in the floodplain spread detected by MODIS. Although HyMAP can simulate interactions between upstream and downstream neighboring grid cells (this includes interactions between major streams and small tributaries) through the local inertia formulation, outflows are unidirectional; hence, it is not currently capable of representing such bifurcations. Consequently, more water is stored in the intermittent lakes in the northeastern area.

As a result of intensified water loss through evapotranspiration in a two-way coupled system, one can observe a significant drop in water extent in 2-WAY outputs, with wet seasons averaging 12,740km^2 (Figure 3c), a 40% drop compared to 1-WAY, and 14% overestimation compared to MODIS, and dry seasons averaging 5750km^2. Compared to 1-WAY, there is an average drop of 5470km^2 regionwide during the 2002-2018 period, in particular, over the central wetlands and over the intermittent lakes (Figure 3f). Monthly water extents derived from 2-WAY shows better correlation with MODIS (r=0.83), when compared to 1-WAY (r=0.74). However, 2-WAY shows a slight degradation in the variability ratio (γ=0.71, as opposed to 0.75 for 1-WAY). It is important to note that all HyMAP grid cells are composed of river reaches with varying geometry and, as long as there is any water flowing in those reaches, grid flooded areas will correspond to the river area that is covered with water. This explains the flood occurrence in all major rivers and numerous small tributaries over the domain in both experiments. MODIS, on the other hand, might miss smaller rivers and streams due to the spatial resolution, and limitations in the sensor and the classification algorithm. These limitations are particularly evident during the dry seasons, where most rivers remain undetected, resulting in low water extent estimates. Also, the spectral properties of mudflats and flood plains in wetlands are similar resulting in misclassification of MODIS flood water extent (Whyte et al., 2018). This means that MODIS estimates could be underestimated and

the actual water extent during dry seasons could be closer to the 2-WAY estimates. That could also result in lower amplitudes for MODIS estimates (i.e., lower standard deviation), leading to better variability ratios.

As opposed to the slight drop in wetland extent previously reported in the literature (Bergé-Nguyen and Crétaux, 2015), our MODIS data classification shows a statistically significant positive trend of ~175km^2/year over annual wet seasons of the study period, as shown in Figure 3g. This trend is in agreement with the previously reported increase in terrestrial water storage over West Africa, as a result of intensified precipitation in the region (Getirana et al., 2020a; Ndehedehe et al., 2016; Rodell et al., 2018). Annual wet-season water extent simulations also show positive trends of 277km^2/year with 1-WAY, and 220km^2/year with 2-WAY, which is in a better agreement with MODIS estimates (Figure 3g).

Impacts of the two-way coupling on surface water dynamics were also evaluated in terms of improvements in water elevation simulations at twelve locations over the Niger River (Figure 1). Biases exist between simulated water elevations and satellite altimetry and are also present between different satellite missions (Calmant et al., 2013; Getirana et al., 2013). In this sense, before comparison, water elevation time series were bias-corrected by removing the long-term mean. Three metrics defined by Equations 6-8 (NS_{NIC}, r_{NIC} and γ_{NIC}) were used to quantify improvements in simulated water level anomalies and results are shown in Figure 4. Most locations (nine or ten out of twelve, depending on the metric) showed improvements, and averaged metrics for all locations were considerably positive: NS_{NIC}=0.58, r_{NIC}=0.65 and γ_{NIC}=0.45. A more detailed interpretation of results at ICESat is limited due to the reduced number of transects (11-15 transects per location). However, the overall improvement suggest that the two-way coupled modeling system improves water level variability, in particular the seasonality. Except for H1, located in the central part of the wetland where the amplitude ratio was degraded, all other Hydrosat locations showed improvements in all metrics.

3.2. Impacts on surface water fluxes

Long-term ET estimates derived from ALEXI, GLEAM and FLUXCOM over flooding zones vary widely, averaging 2.5, 1 and 1.5 mm/day, respectively. Such an uncertainty has been previously described in the literature (H. C. Jung et al., 2019) and is visible in the maps illustrated in Figures 5a-c. All three satellite-based ET estimates show a northward drop caused by a climate gradient as

a result of West African monsoons (Boone et al., 2009). Both ALEXI and FLUXCOM can detect higher ET rates over the wetland, although ALEXI gives significantly higher rates than FLUXCOM. Due to this high ET uncertainty over the region, we chose to evaluate model outputs against the mean of these three satellite-based estimates, which averages 1.69mm/day over flooding zones.

Noah-MP is capable of representing the northward evapotranspiration gradient observed in the other products, but it underestimates ET rates over flooding zones, averaging 0.79mm/day (see Figure 5d). Recent studies show that Noah-MP generally underestimates ET over West Africa compared to other models and satellite-based estimates (H. C. Jung et al., 2019). The resulting ET derived from the 2-WAY experiment shows clear patterns of modeled rivers and flooded areas and significantly higher evapotranspiration rates, averaging 1.57mm/day over flooding zones. Figure 6 shows the temporal variability of evapotranspiration over flooding zones derived from model experiments and estimate averages. Simulated ET estimates during wet seasons derived from the 1-WAY experiment are generally well represented when compared to satellite-based estimates with slight underestimation. Its large bias is mostly caused by the substantial underestimation during dry seasons, with monthly average rates over flooding zones as low as 0.1 mm/day. As a result, ET derived from 1-WAY has a negative bias of -0.9mm/day, high variability ratio with γ=1.28 and low NS value of -0.89. Accounting for surface water availability in the vertical water balance considerably increases ET rates during dry seasons to values between 0.8 and 1.6mm/day, depending on the year, and slightly increases rates during wet seasons. These changes lead to an improved bias of 0.1mm/day, as well as variability ratio, with γ=0.9, and NS=0.86. Two-way coupling showed was virtually no impact on ET timing, with similar correlation values for both experiments (0.96 and 0.94 for 1-WAY and 2-WAY, respectively).

Two-meter layer soil moisture significantly increases with higher surface water infiltration rates, in particular over flooding zones where top soil layers reach saturation during the wet seasons, as shown in Figures 7a-b. On average, soil moisture increases 50mm with largest differences during dry seasons. frequent rainfall during wet seasons results in smaller differences between soil moisture of both experiments. Wetter soils allow higher latent heat flux rates associated with evaporation, reducing surface temperatures over flooding zones by, on average, 1.2ºC (see Figures 7c-d). However, permanently flooded areas show averaged surface temperature drops of 7ºC over the study period. The double peaked surface temperature cycle follows the regional air temperature

seasonality, with the highest peak occurring in May and second one in October. Largest differences in surface temperature occur during these peaks, and account for two-way coupling results a slight flattening of the second peak. Figures 7e-f shows spatial and temporal changes in surface water storage (SWS) when two-way coupling is accounted for. On average, SWS drops ~137mm over flooding zones, with minimum and maximum drops occurring in September (90mm) and January (175mm), respectively.

As shown in Figure 8, Streamflow simulations from the 1-WAY experiment over 2002-2012 overestimate observations by 77%, totaling 1648m^3/s, and flood peaks are delayed, on average, by 33 days (DI=-33). Such a bias and lag resulted in a low Nash-Sutcliffe of -0.78. The variability of streamflow observations and derived from the 1-WAY experiment are similar, indicated by the variability ratio γ of 1.06. Streamflow simulations are substantially improved when surface water becomes available to the LSM vertical water balance in the 2-WAY experiment. Average river discharge derived from 2-WAY is 1048m^3/s, indicating an average water loss rate of 600m^3/s (or ~18,900km^3/year) from wetlands to the atmosphere, in addition to the evapotranspiration computed in the 1-WAY experiment. Bias and DI drop to 214m^3/s (i.e., 20% overestimation compared to the observed average) and -16 days, respectively, resulting in a meaningful Nash-Sutcliffe improvement to 0.79. The variability remained basically the same, with γ=1.04. Based on these results, it is reasonable to assume that the lag and bias detected downstream the wetland is explained by misrepresented interactions of surface waters with land surface and atmosphere. Without a proper hydrological coupling between models, surface water storage is overestimated as a result of the neglection of its infiltration to the soil and evaporation to the atmosphere. The excess water is stored in floodplains, resulting in delayed flood peaks downstream the wetland.

4. Summary

This paper describes a new framework for the two-way coupling between LSMs and flood models in NASA's Land Information System and evaluates its impacts on key hydrological variables in the Inner Niger Delta. Here, the surface water dynamics computed by HyMAP was accounted for in Noah-MP's vertical water and energy balance and results were compared against an experiment where such processes are neglected. We found that the wetland has a major role in soil moisture and evapotranspiration rates that result in a major water loss rate from the surface to the

atmosphere. Such a water loss accounts for a substantial decline in both water extent and wetland outflow.

For over ten years, different studies found in the literature describe the implementation and improvement of two-way coupling approaches and, undoubtedly, they all have paved the way for the current and future generations of Earth system models. The large majority, however, represents surface water dynamics through very simplified schemes and overcome the limited representation of floodplains by using coarse spatial resolutions from 0.125º to 1º. There is a consensus that better surface water parameterizations are needed for a more accurate representation of interactions between wetlands and the land surface (e.g., Chaney et al., 2020; Miguez-Macho and Fan, 2012b). Using the local inertia formulation in HyMAP allowed us to represent wetland dynamics at a significantly finer spatial resolution (i.e., 0.02º) and the spatially distributed impacts on the water and energy balances. It is important to note that this implementation can be expanded to the suite of LSMs available in LIS, as well as used in conjunction with its data assimilation schemes (e.g., Kumar et al., 2019, 2015b, 2020, 2016; Li et al., 2019). These advantages could be an asset to current LIS-based water monitoring systems (e.g., Arsenault et al., 2020; Getirana et al., 2020c; Kumar et al., 2019; McNally et al., 2019; Rodell et al., 2004).

Beside these advantages, the proposed modeling system has a number of limitations. For example, the current HyMAP parameterization neglects bifurcation. Such a process has been shown to be essential in large-scale flood modeling for a more accurate representation of lateral water distribution over flat areas and deltas (Yamazaki et al., 2014). Although MERIT DEM, where some of the HyMAP parameters were derived from, shows improvement in representing global topography, it is still not free from errors that could result in the misrepresentation of parameters, such as flow directions, slope, river length, floodplain extent and water storage, in particular in flat areas such as IND. HyMAP river geometry is still heavily based on empirical equations, which is another possible source of errors that could impact the simulation of wetland dynamics. MERIT-Hydro was used here as an attempt to minimize river geometry uncertainty, but river width estimates are only available for major rivers. Besides, MERIT-Hydro has its own uncertainties related to Landsat spatial resolution and the land cover classification algorithms. The misrepresentation of the aforementioned physical processes geomorphological characteristics may have a meaningful impact on the vertical water and energy balance computed by Noah-MP in a two-way coupled modeling system and might have contributed to the wetland extent mismatch

between MODIS estimates and model outputs. In this sense, it is strongly suggested that future work focus on the development of improved representation of surface water dynamics (e.g., Neal et al., 2012) that can be further used in two-way coupled modeling systems. Floodplain and wetland modeling can also be improved through satellite data assimilation. Recent work has shown that assimilating satellite-based water extent (Hostache et al., 2018), radar altimetry and streamflow observations (Paiva et al., 2013a) significantly improves surface water dynamic modeling. Solutions could envisage the simultaneous assimilation of these observations, also called multivariate data assimilation (Kumar et al., 2019), optimizing their synergetic impacts on the representation of multiple hydrological variables. Finally, while our broad conclusions about the impacts of two-way coupling on the water cycle modeling are likely to be true, as endorsed by similar studies, we caution that the precise quantities reported would likely change if the modeling configuration (LSM, routing scheme, and meteorological forcing data set) were different. However, further investigation considering different modeling approaches would provide additional insight.

Acknowledgements

The MERRA-2 meteorological dataset is distributed by the Goddard Earth Sciences (GES) Data and Information Services Center (DISC; https://earthdata.nasa.gov/about/daacs/daac-ges-disc). CHIRPS rainfall estimates are made available by the Climate Hazards Center at UC Santa Barbara through https://www.chc.ucsb.edu/data/chirps/ website. Eight-day surface spectral reflectance MODIS data products are made available through https://lpdaac.usgs.gov/products/mod09a1v006/. Streamflow data are collected by different national water services, assembled by the *Comité permanent Inter état de Lutte contre la Sécheresse au Sahel* (CILSS) and available under request. Radar altimetry data is available through the Hydrosat website (http://hydrosat.gis.uni-stuttgart.de/php/index.php) and ICESat-2 data through OpenAltimetry (https://openaltimetry.org). Satellite-based evapotranspiration estimates are available through the GLEAM (https://www.gleam.eu) and FLUXCOM (http://www.fluxcom.org) websites. LIS Framework is available on https://github.com/NASA-LIS/LISF. Computing resources supporting this work were provided by the NASA High-End Computing (HEC) Program through the NASA Center for Climate Simulation (NCCS) at NASA's Goddard Space Flight Center. This study was funded by NASA's Terrestrial Hydrology Program. The authors would like to thank M. Tourian for his support on using the Hydrosat database.

Appendix

A.1. Inflow at Niger and Beni Rivers

The Niger inner delta model was constrained upstream the delta, over the Niger and Beni Rivers, streamflow simulations derived from an existing hydrological model for the whole Niger basin, as described in Getirana et al. (2020a). The model run is composed of HyMAP one-way coupled with the Catchment Land Surface Model (CLSM; Koster et al., 2000) at 0.25° spatial resolution and 15-min time step. In order to minimize errors in the simulated streamflow used as boundary condition for the Niger inner delta model, daily streamflow observations at Koulikoro and Pankourou (see Table 1 for details) are directly inserted in the model and propagated through the river network. The time series is completed with bias-corrected simulations, using a polynomial regression equation defined for the period where observations are available. Streamflow simulations at locations defined in Figure 1 as Niger and Bani inflows are used as boundary conditions in the proposed Inner Niger Delta modeling.

586 **Tables**

587 **Table 1**: List of gauging stations in the Niger River basin considered in this study. Drainage areas
588 are derived from HyMAP parameters. Values provided by agencies, when available, are also listed.
589 Average streamflow is provided for the study period (2002-2018), as a function of data availability.

Gauging station	River	Basin	Country	Longitude	Latitude	Drain. area [km^2]	Avg. streamflow [m^3/s]	Flood peak [months]	Data availability [years]
Diré	Niger	Niger	Mali	-3.9	16.3	362,280	845	10-12	1950-2012
Ké Macina	Niger	Niger	Mali	-5.4	14	137,150	896	8-10	1953-2007
Koulikoro	Niger	Niger	Mali	-7.6	12.9	120,000	1086	8-10	1950-2012
Pankourou	Bagoe	Niger	Mali	-6.6	11.4	35,080	131	8-10	1956-2013

590

591 **Table 2:** Noah-MP options adopted in this study to represent physical processes.

Physical process	**Noah-MP 4.0.1 options**	**References**
Vegetation	Monthly climatology of leaf area index (LAI) and albedo used to represent vegetation dynamic (Option 4)	Niu et al (2011)
Stomatal resistance	Ball-Berry (Option 1)	Ball et al (1987)
Soil moisture factor for stomatal resistance	Noah-type based on soil moisture (Option 1)	Chen et al (1996)
Runoff & groundwater	SIMGM: based on TOPMODEL (Option 1)	Niu et al. (2007)
Surface layer drag coefficient	Monin-Obukhov (Option 1)	Monin and Obukhov (1954)
Radiation transfer	Modified two-stream scheme (Option 1)	Niu and Yang (2004)

592 *Note: Cold-season related processes and options (e.g., snow fall, accumulation and depth) are not included here.*
593

Figures

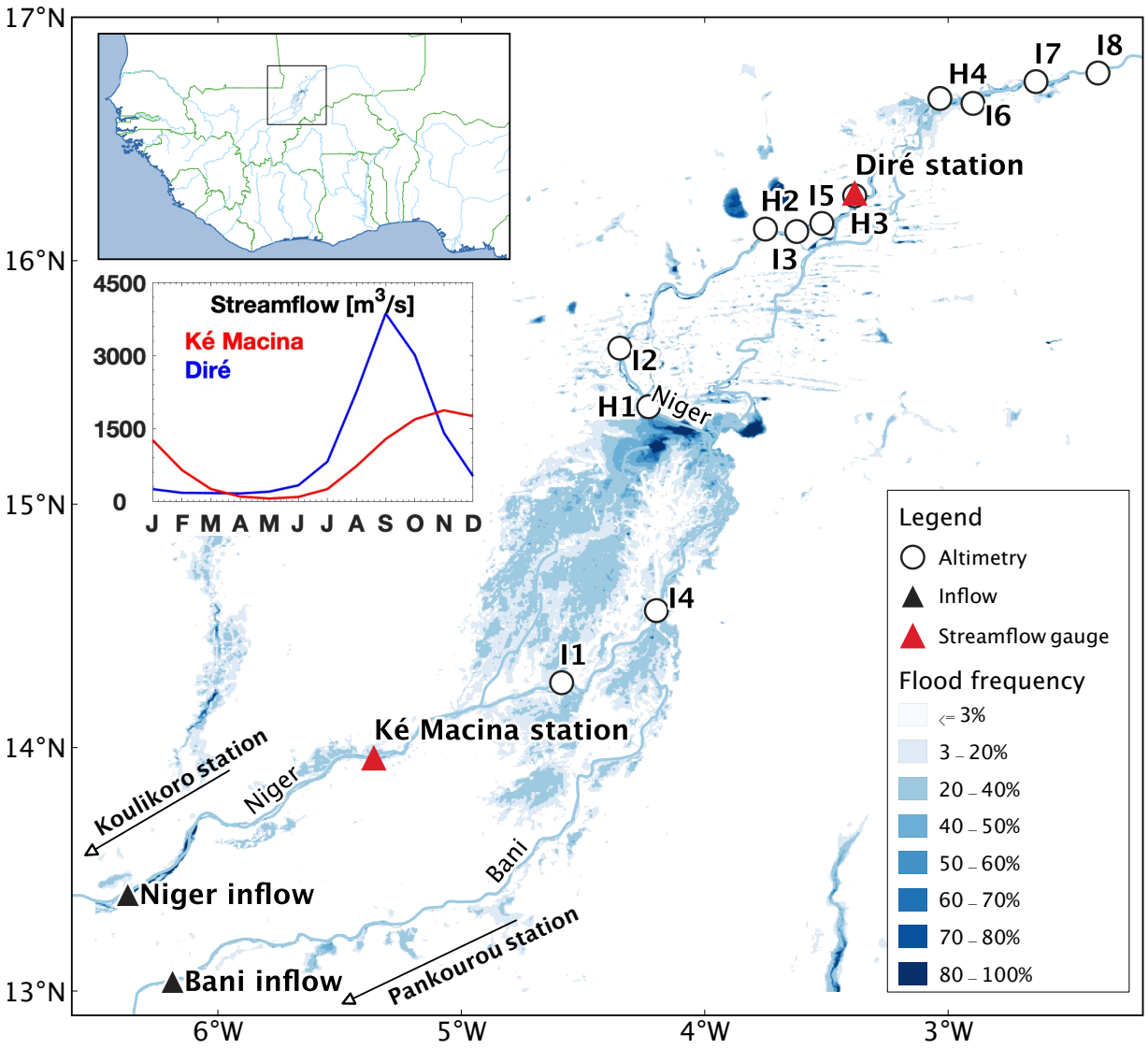

Figure 1: Niger inner delta geographic location and data availability. Circles indicate locations where radar and laser altimeter orbits transect the Niger River (I1-I8 and H1-H4 stand for ICESat and Hydrosat datasets, respectively) and the red triangle shows the gauging station where daily streamflow data is available for evaluation. Black triangles indicate where daily inflows were used as boundary conditions for modeling experiments. The flood occurrence map is derived from 250-meter MODIS observations over the 2002-2018 period. Monthly climatologies of streamflow observations at Ké Mecina and Diré stations are also illustrated.

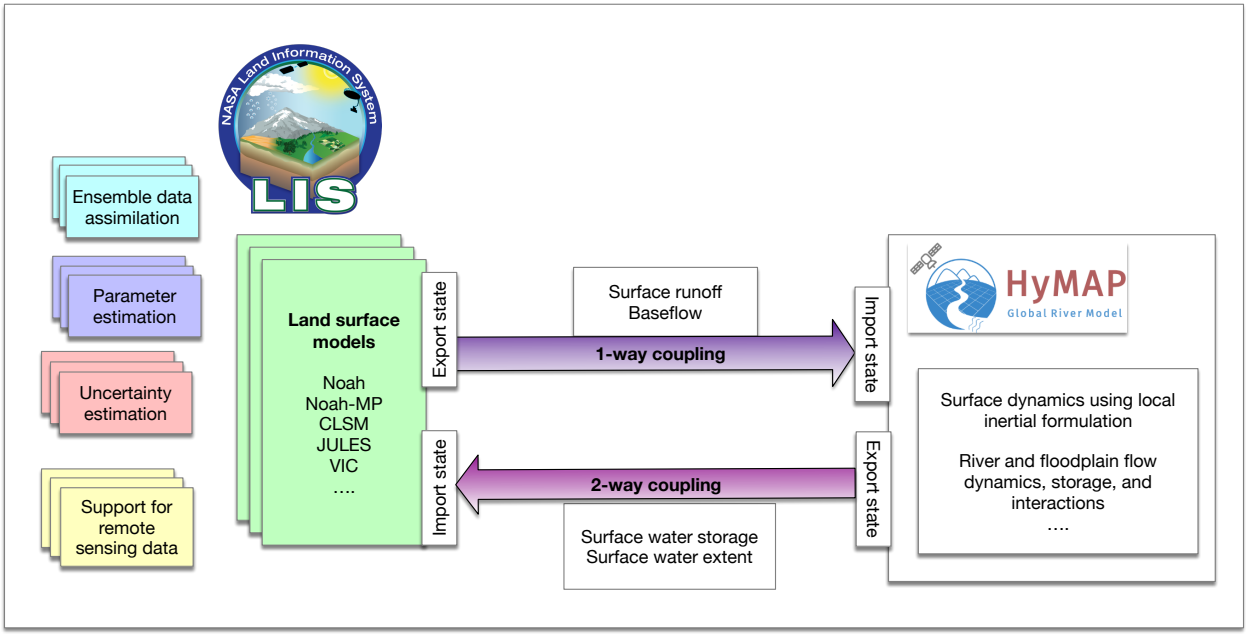

603

604 **Figure 2:** NASA's Land Information System (LIS) model coupling schematic. One and two-way
605 coupling between HyMAP and LSMs use standardized software tools and paradigms enabled by
606 the Earth System Modeling Framework.

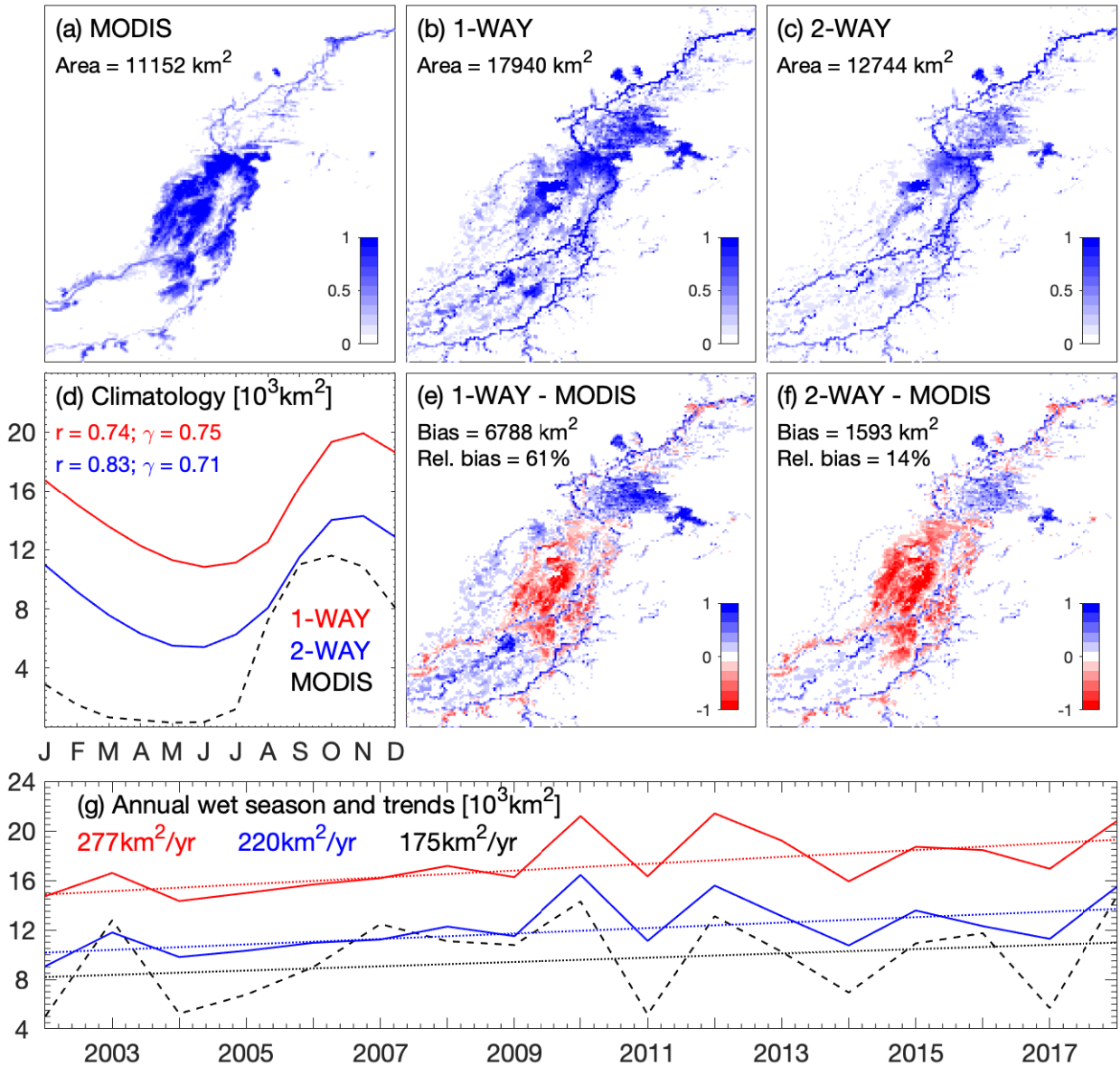

607

608 **Figure 3:** Niger inner delta flooded fraction averaged over 2002-2018 wet seasons (April-June)
609 (a) estimated from MODIS observations, derived from (b) one-way and (c) two-way coupled land
610 surface-flood modeling experiments, (d) their monthly climatology. Panels (e) and (f) show
611 differences between wet-season long-term averaged model simulations and satellite estimates, and
612 (g) the annual wet-season water extent averages and trends. To facilitate the spatial comparison,
613 the 250-meter MODIS data was upscaled to a 0.02º flooded fraction map.

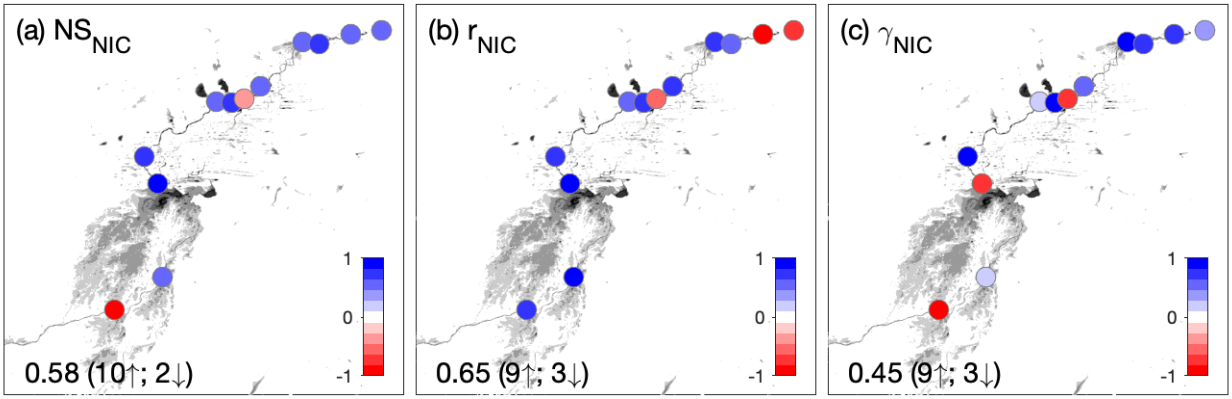

614

615 **Figure 4:** Normalized improved coefficients (NIC) of (a) Nash-Sutcliffe, (b) correlation and (c)
616 variability ratio for unbiased river water elevations derived from one-way and two-way coupled
617 land surface-flood modeling experiments. Metrics are defined in Eqs. (6)-(8) and computed for
618 variable time periods within 2002-2018, as a function of data availability at each location.

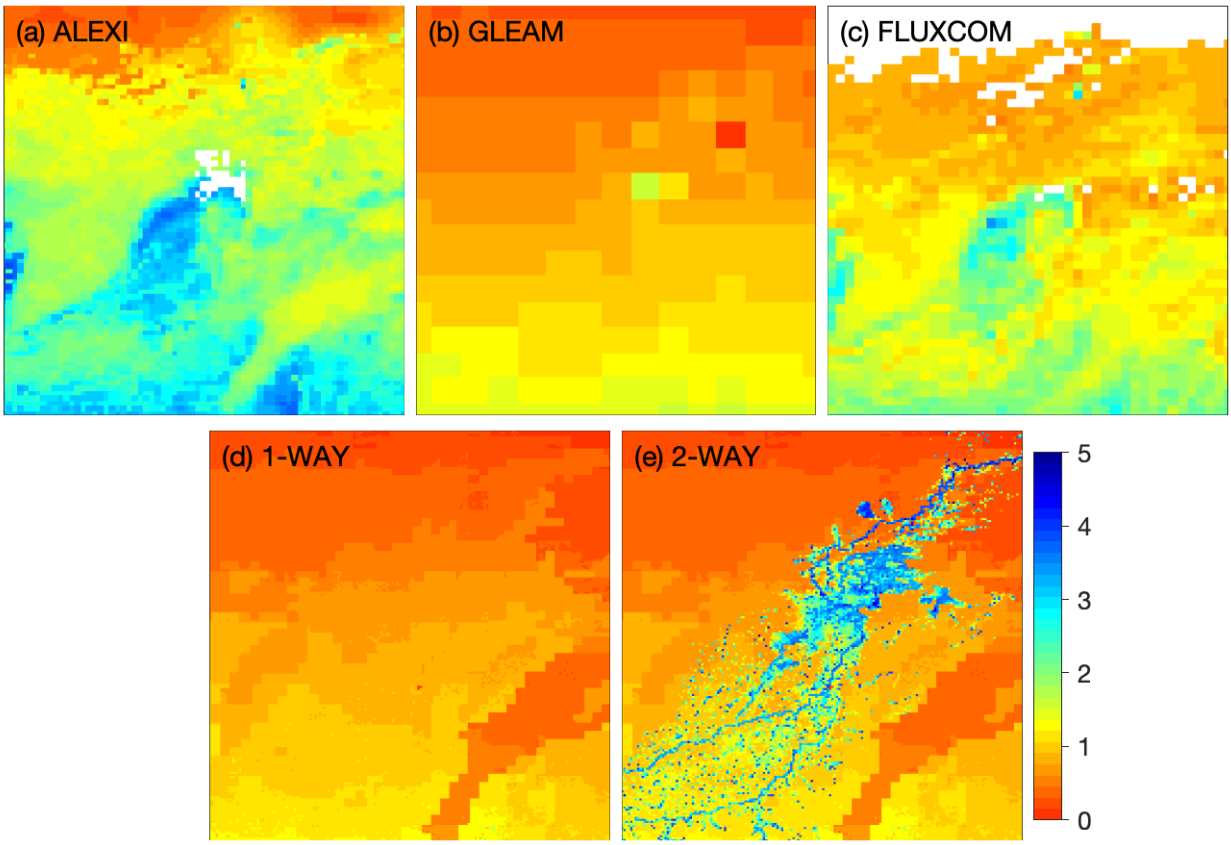

619

620 **Figure 5:** Spatially distributed evapotranspiration rates [mm/day] derived from (a) ALEXI, (b)
621 GLEAM, (c) FLUXCOM, (d) one-way coupling experiment (1-WAY) and (e) two-way coupling
622 experiment (2-WAY). Rates are averages over 2002-2015.

623

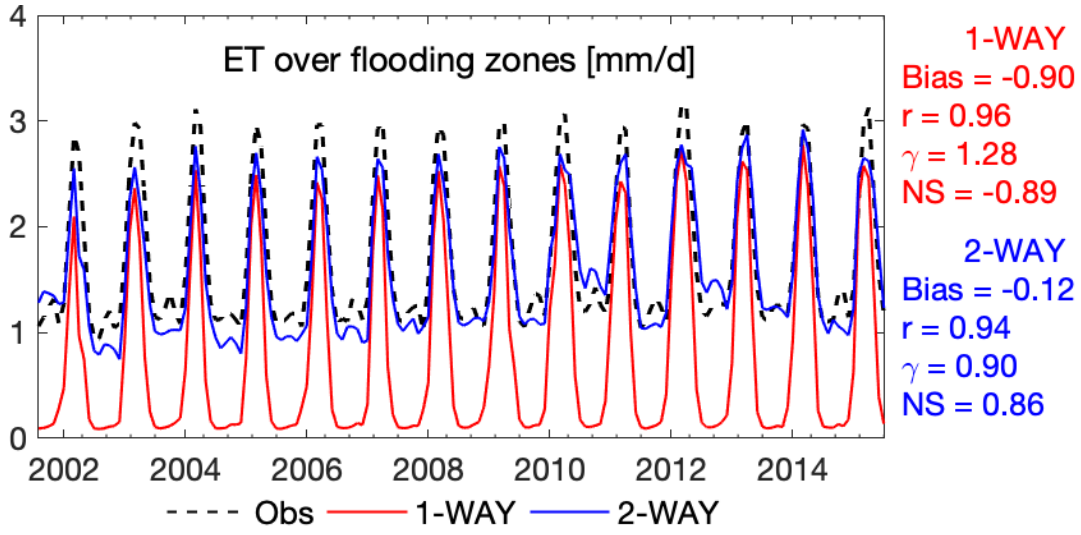

624

625 **Figure 6:** Modeled and satellite-based total evapotranspiration (ET) time series over flooding
626 zones for the 2002-2015 period, where all datasets overlap. Simulations are derived from one-way
627 and two-way coupled land surface-flood modeling experiments. Obs stands for the mean of
628 ALEXI, GLEAMv3.3a and FLUXCOM satellite-based ET products. The following metrics are
629 provided for each modeling experiment: bias, correlation (r), variability ratio (γ) and Nash-
630 Sutcliffe (NS) coefficient.

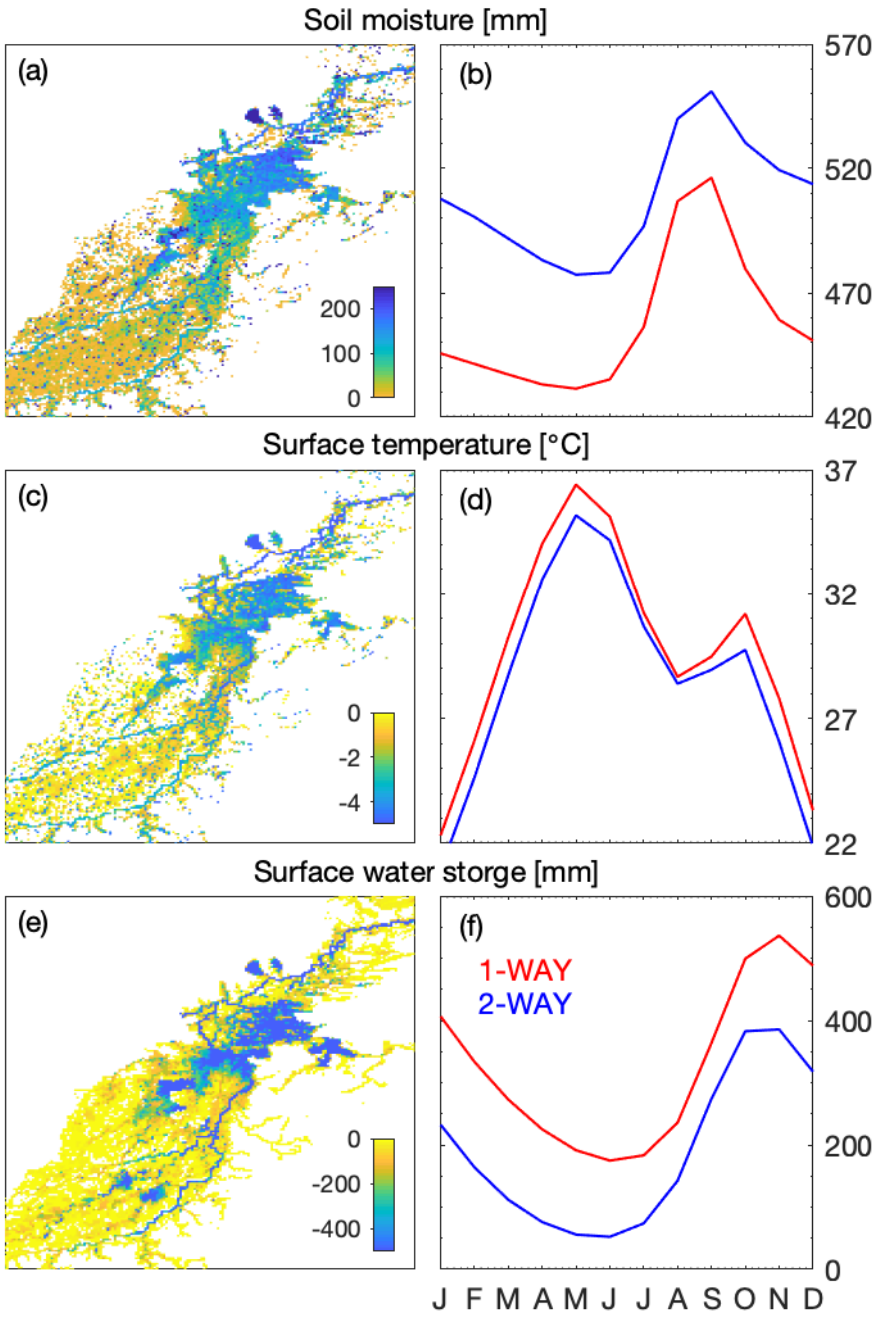

631

632 **Figure 7:** Panels on the left show impacts of two-way coupling over the Niger inner delta on
633 spatially distributed (a) soil moisture, (b) surface temperature and (c) surface water storage.
634 Impacts are defined here as the long-term difference between two-way and one-way coupling
635 experiments, i.e., 2-WAY - 1-WAY. Panels on the right show monthly climatologies of
636 corresponding spatially-averaged variables over flooding zones.

637

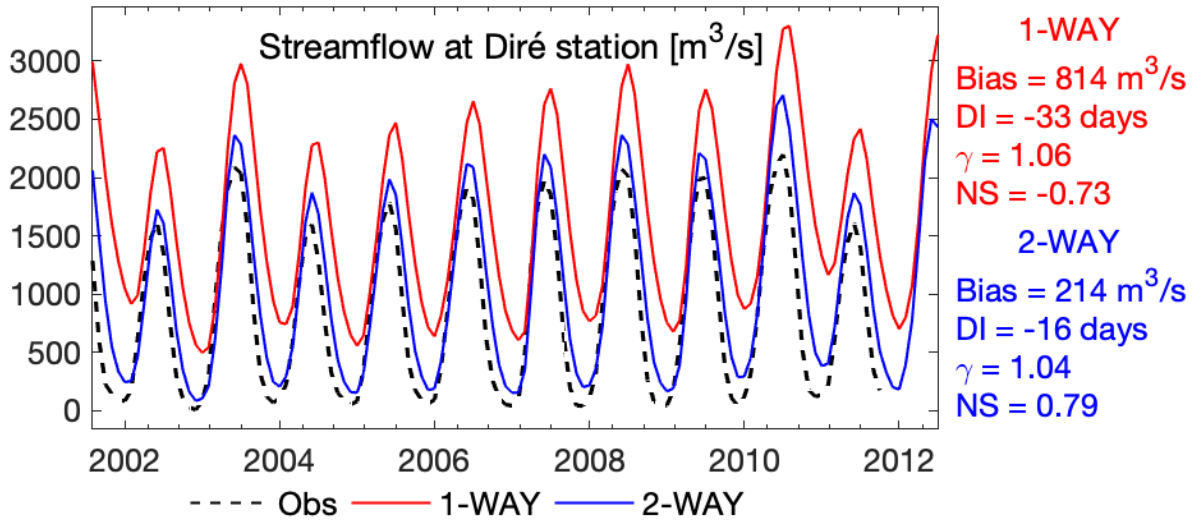

638

639 **Figure 8:** Simulated and observed streamflow time series at Diré gauging station over the 2002-
640 2012 period. Simulations are derived from one-way and two-way coupled land surface-flood
641 modeling experiments. Selected metrics are provided for each modeling experiment: bias, delay
642 index (DI), variability ratio (γ) and Nash-Sutcliffe (NS) coefficient.

References

Anderson, M.C., Norman, J.M., Mecikalski, J.R., Otkin, J.A., Kustas, W.P., 2007. A climatological study of evapotranspiration and moisture stress across the continental United States based on thermal remote sensing: 1. Model formulation. J. Geophys. Res. Atmos. 112. https://doi.org/10.1029/2006JD007506

Arsenault, K.R., Kumar, S. V., Geiger, J. V., Wang, S., Kemp, E., Mocko, D.M., Beaudoing, H.K., Getirana, A., Navari, M., Li, B., Jacob, J., Wegiel, J., Peters-Lidard, C.D., 2018. The Land surface Data Toolkit (LDT v7.2) - A data fusion environment for land data assimilation systems. Geosci. Model Dev. 11, 3605–3621. https://doi.org/10.5194/gmd-11-3605-2018

Arsenault, K.R., Shukla, S., Hazra, A., Getirana, A., McNally, A., Kumar, S. V., Koster, R.D., Peters-Lidard, C.D., Zaitchik, B.F., Badr, H., Jung, H.C., Narapusetty, B., Navari, M., Wang, S., Mocko, D.M., Funk, C., Harrison, L., Husak, G.J., Adoum, A., Galu, G., Magadzire, T., Roningen, J., Shaw, M., Eylander, J., Bergaoui, K., McDonnell, R.A., Verdin, J.P., 2020. The NASA hydrological forecast system for food and water security applications. Bull. Am. Meteorol. Soc. BAMS-D-18-0264.1. https://doi.org/10.1175/BAMS-D-18-0264.1

Ball, J.T., Woodrow, I.E., Berry, J.A., 1987. A Model Predicting Stomatal Conductance and its Contribution to the Control of Photosynthesis under Different Environmental Conditions, in: Progress in Photosynthesis Research. Springer Netherlands, Dordrecht, pp. 221–224. https://doi.org/10.1007/978-94-017-0519-6_48

Bates, P.D., Horritt, M.S., Fewtrell, T.J., 2010. A simple inertial formulation of the shallow water equations for efficient two-dimensional flood inundation modelling. J. Hydrol. 387, 33–45. https://doi.org/10.1016/j.jhydrol.2010.03.027

Bergé-Nguyen, M., Crétaux, J.-F., 2015. Inundations in the Inner Niger Delta: Monitoring and Analysis Using MODIS and Global Precipitation Datasets. Remote Sens. 7, 2127–2151. https://doi.org/10.3390/rs70202127

Bichet, A., Diedhiou, A., 2018. West African Sahel has become wetter during the last 30 years, but dry spells are shorter and more frequent. Clim. Res. 75, 155–162. https://doi.org/10.3354/cr01515

Bonafilia, D., Tellman, B., Anderson, T., Issenberg, E., 2020. Sen1Floods11: a georeferenced dataset to train and test deep learning flood algorithms for Sentinel-1, in: 2020 IEEE/CVF Conference on Computer Vision and Pattern Recognition Workshops (CVPRW). IEEE, pp. 835–845. https://doi.org/10.1109/CVPRW50498.2020.00113

Boone, A., de Rosnay, P., Balsamo, G., Beljaars, A., Chopin, F., Decharme, B., Delire, C., Ducharne, A., Gascoin, S., Grippa, M., Guichard, F., Gusev, Y., Harris, P., Jarlan, L., Kergoat, L., Mougin, E., Nasonova, O., Norgaard, A., Orgeval, T., Ottlé, C., Poccard-Leclercq, I., Polcher, J., Sandholt, I., Saux-Picart, S., Taylor, C., Xue, Y., 2009. The AMMA Land Surface Model Intercomparison Project (ALMIP). Bull. Am. Meteorol. Soc.

90, 1865–1880. https://doi.org/10.1175/2009BAMS2786.1

Calmant, S., da Silva, J.S., Moreira, D.M., Seyler, F., Shum, C.K., Crétaux, J.F., Gabalda, G., 2013. Detection of Envisat RA2/ICE-1 retracked radar altimetry bias over the Amazon basin rivers using GPS. Adv. Sp. Res. 51, 1551–1564. https://doi.org/10.1016/j.asr.2012.07.033

Chaney, N.W., Torres-rojas, L., Vergopolan, N., Fisher, C.K., 2020. GMDD - Two-way coupling between the sub-grid land surface and river networks in Earth system models 1–31.

Chen, F., Mitchell, K., Schaake, J., Xue, Y., Pan, H.-L., Koren, V., Duan, Q.Y., Ek, M., Betts, A., 1996. Modeling of land surface evaporation by four schemes and comparison with FIFE observations. J. Geophys. Res. Atmos. 101, 7251–7268. https://doi.org/10.1029/95JD02165

Cox, P.M., Betts, R.A., Bunton, C.B., Essery, R.L.H., Rowntree, P.R., Smith, J., 1999. The impact of new land surface physics on the GCM simulation of climate and climate sensitivity. Clim. Dyn. 15, 183–203. https://doi.org/10.1007/s003820050276

Csiszar, I., Gutman, G., 1999. Mapping global land surface albedo from NOAA AVHRR. J. Geophys. Res. Atmos. 104, 6215–6228. https://doi.org/10.1029/1998JD200090

Dadson, S.J., Ashpole, I., Harris, P., Davies, H.N., Clark, D.B., Blyth, E., Taylor, C.M., 2010. Wetland inundation dynamics in a model of land surface climate: Evaluation in the Niger inland delta region. J. Geophys. Res. 115, D23114. https://doi.org/10.1029/2010JD014474

De Almeida, G.A.M., Bates, P., Freer, J.E., Souvignet, M., 2012. Improving the stability of a simple formulation of the shallow water equations for 2-D flood modeling. Water Resour. Res. 48, 1–14. https://doi.org/10.1029/2011WR011570

Decharme, B., Alkama, R., Papa, F., Faroux, S., Douville, H., Prigent, C., 2012. Global off-line evaluation of the ISBA-TRIP flood model. Clim. Dyn. 38, 1389–1412. https://doi.org/10.1007/s00382-011-1054-9

Decharme, B., Delire, C., Minvielle, M., Colin, J., Vergnes, J., Alias, A., Saint-Martin, D., Séférian, R., Sénési, S., Voldoire, A., 2019. Recent Changes in the ISBA-CTRIP Land Surface System for Use in the CNRM-CM6 Climate Model and in Global Off-Line Hydrological Applications. J. Adv. Model. Earth Syst. 11, 1207–1252. https://doi.org/10.1029/2018MS001545

Dembélé, M., Zwart, S.J., 2016. Evaluation and comparison of satellite-based rainfall products in Burkina Faso, West Africa. Int. J. Remote Sens. 37, 3995–4014. https://doi.org/10.1080/01431161.2016.1207258

Dinku, T., Funk, C., Peterson, P., Maidment, R., Tadesse, T., Gadain, H., Ceccato, P., 2018. Validation of the CHIRPS satellite rainfall estimates over eastern Africa. Q. J. R. Meteorol. Soc. 144, 292–312. https://doi.org/10.1002/qj.3244

Ek, M.B., Mitchell, K.E., Lin, Y., Rogers, E., Grunmann, P., Koren, V., Gayno, G., Tarpley, J.D., 2003. Implementation of Noah land surface model advances in the National Centers

for Environmental Prediction operational mesoscale Eta model. J. Geophys. Res. Atmos. 108. https://doi.org/10.1029/2002JD003296

Farr, T.G., Rosen, P.A., Caro, E., Crippen, R., Duren, R., Hensley, S., Kobrick, M., Paller, M., Rodriguez, E., Roth, L., Seal, D., Shaffer, S., Shimada, J., Umland, J., Werner, M., Oskin, M., Burbank, D., Alsdorf, D., 2007. The Shuttle Radar Topography Mission. Rev. Geophys. 45. https://doi.org/10.1029/2005RG000183

Funk, C., Peterson, P., Landsfeld, M., Pedreros, D., Verdin, J., Shukla, S., Husak, G., Rowland, J., Harrison, L., Hoell, A., Michaelsen, J., 2015. The climate hazards infrared precipitation with stations - A new environmental record for monitoring extremes. Sci. Data 2, 1–21. https://doi.org/10.1038/sdata.2015.66

Getirana, A., Bonnet, M.-P., Martinez, J.-M., 2009a. Evaluating parameter effects in a DEM "burning" process based on land cover data. Hydrol. Process. 23. https://doi.org/10.1002/hyp.7303

Getirana, A., Bonnet, M.-P., Rotunno Filho, O.C., Mansur, W.J., 2009b. Improving hydrological information acquisition from DEM processig in floodplains. Hydrol. Process. 23. https://doi.org/10.1002/hyp.7167

Getirana, A., Boone, A., Yamazaki, D., Mognard, N., 2013. Automatic parameterization of a flow routing scheme driven by radar altimetry data : Evaluation in the Amazon basin. Water Resour. Res. 49. https://doi.org/10.1002/wrcr.20077

Getirana, A., Dutra, E., Guimberteau, M., Kam, J., Li, H.Y., Decharme, B., Zhang, Z., Ducharne, A., Boone, A., Balsamo, G., Rodell, M., Toure, A.M., Xue, Y., Peters-Lidard, C.D., Kumar, S. V., Arsenault, K., Drapeau, G., Leung, L.R., Ronchail, J., Sheffield, J., 2014. Water balance in the amazon basin from a land surface model ensemble. J. Hydrometeorol. 15, 2586–2614. https://doi.org/10.1175/JHM-D-14-0068.1

Getirana, A., Jung, H.C., Arsenault, K., Shukla, S., Kumar, S., Peters-Lidard, C., Maigari, I., Mamane, B., 2020a. Satellite gravimetry improves seasonal streamflow forecast initialization in Africa. Water Resour. Res. 2019WR026259. https://doi.org/10.1029/2019WR026259

Getirana, A., Jung, H.C., Van Den Hoek, J., Ndehedehe, C.E., 2020b. Hydropower dam operation strongly controls Lake Victoria's freshwater storage variability. Sci. Total Environ. 726, 138343. https://doi.org/10.1016/j.scitotenv.2020.138343

Getirana, A., Kumar, S., Girotto, M., Rodell, M., 2017a. Rivers and Floodplains as Key Components of Global Terrestrial Water Storage Variability. Geophys. Res. Lett. 44, 10,359-10,368. https://doi.org/10.1002/2017GL074684

Getirana, A., Peters-Lidard, C., 2013. Estimating water discharge from large radar altimetry datasets. Hydrol. Earth Syst. Sci. 17. https://doi.org/10.5194/hess-17-923-2013

Getirana, A., Peters-Lidard, C., Rodell, M., Bates, P.D., 2017b. Trade-off between cost and accuracy in large-scale surface water dynamic modeling. Water Resour. Res.

https://doi.org/10.1002/2017WR020519

Getirana, A., Rodell, M., Kumar, S., Beaudoing, H.K., Arsenault, K., Zaitchik, B., Save, H., Bettadpur, S., 2020c. GRACE Improves Seasonal Groundwater Forecast Initialization over the United States. J. Hydrometeorol. 21, 59–71. https://doi.org/10.1175/JHM-D-19-0096.1

Getirana, A.C.V., Boone, A., Yamazaki, D., Decharme, B., Papa, F., Mognard, N., 2012. The hydrological modeling and analysis platform (HyMAP): Evaluation in the Amazon basin. J. Hydrometeorol. 13, 1641–1665. https://doi.org/10.1175/JHM-D-12-021.1

Gimeno, L., Drumond, A., Nieto, R., Trigo, R.M., Stohl, A., 2010. On the origin of continental precipitation. Geophys. Res. Lett. 37, n/a-n/a. https://doi.org/10.1029/2010GL043712

Hain, C.R., Anderson, M.C., 2017. Estimating morning change in land surface temperature from MODIS day/night observations: Applications for surface energy balance modeling. Geophys. Res. Lett. 44, 9723–9733. https://doi.org/10.1002/2017GL074952

Hill, C., DeLuca, C., Balaji, Suarez, M., Da Silva, A., 2004. The architecture of the earth system modeling framework. Comput. Sci. Eng. 6, 18–28. https://doi.org/10.1109/MCISE.2004.1255817

Hostache, R., Chini, M., Giustarini, L., Neal, J., Kavetski, D., Wood, M., Corato, G., Pelich, R.M., Matgen, P., 2018. Near-Real-Time Assimilation of SAR-Derived Flood Maps for Improving Flood Forecasts. Water Resour. Res. 54, 5516–5535. https://doi.org/10.1029/2017WR022205

James, G.K., Adegoke, J.O., Saba, E., Nwilo, P., Akinyede, J., 2007. Satellite-Based Assessment of the Extent and Changes in the Mangrove Ecosystem of the Niger Delta. Mar. Geod. 30, 249–267. https://doi.org/10.1080/01490410701438224

Jung, H.C., Getirana, A., Arsenault, K.R., Holmes, T.R.H., McNally, A., 2019. Uncertainties in evapotranspiration estimates over West Africa. Remote Sens. 11. https://doi.org/10.3390/rs11080991

Jung, H.C., Getirana, A., Policelli, F., McNally, A., Arsenault, K.R., Kumar, S., Tadesse, T., Peters-Lidard, C.D., 2017. Upper Blue Nile basin water budget from a multi-model perspective. J. Hydrol. 555, 535–546. https://doi.org/10.1016/j.jhydrol.2017.10.040

Jung, M., Koirala, S., Weber, U., Ichii, K., Gans, F., Camps-Valls, G., Papale, D., Schwalm, C., Tramontana, G., Reichstein, M., 2019. The FLUXCOM ensemble of global land-atmosphere energy fluxes. Sci. Data 6, 74. https://doi.org/10.1038/s41597-019-0076-8

Koster, R.D., Suarez, M.J., Ducharne, A., Stieglitz, M., Kumar, P., 2000. A catchment-based approach to modeling land surface processes in a general circulation model: 1. Model structure. J. Geophys. Res. Atmos. 105, 24809–24822. https://doi.org/10.1029/2000JD900327

Krinner, G., Viovy, N., de Noblet-Ducoudré, N., Ogée, J., Polcher, J., Friedlingstein, P., Ciais, P., Sitch, S., Prentice, I.C., 2005. A dynamic global vegetation model for studies of the coupled atmosphere-biosphere system. Global Biogeochem. Cycles 19.

https://doi.org/10.1029/2003GB002199

Kumar, S., Jasinski, M., Mocko, D.M., Rodell, M., Borak, J., Li, B., Beaudoing, H.K., Peters-Lidard, C.D., 2019. NCA-LDAS Land Analysis: Development and Performance of a Multisensor, Multivariate Land Data Assimilation System for the National Climate Assessment. J. Hydrometeorol. 20, 1571–1593. https://doi.org/10.1175/JHM-D-17-0125.1

Kumar, S., Peters-Lidard, C.D., Arsenault, K.R., Getirana, A., Mocko, D., Liu, Y., 2015a. Quantifying the Added Value of Snow Cover Area Observations in Passive Microwave Snow Depth Data Assimilation. J. Hydrometeorol. 16, 1736–1741. https://doi.org/10.1175/jhm-d-15-0021.1

Kumar, S., Peters-Lidard, C.D., Santanello, J.A., Reichle, R.H., Draper, C.S., Koster, R.D., Nearing, G., Jasinski, M.F., 2015b. Evaluating the utility of satellite soil moisture retrievals over irrigated areas and the ability of land data assimilation methods to correct for unmodeled processes. Hydrol. Earth Syst. Sci. 19, 4463–4478. https://doi.org/10.5194/hess-19-4463-2015

Kumar, S. V., Holmes, T.R., Bindlish, R., de Jeu, R., Peters-Lidard, C., 2020. Assimilation of vegetation optical depth retrievals from passive microwave radiometry. Hydrol. Earth Syst. Sci. 24, 3431–3450. https://doi.org/10.5194/hess-24-3431-2020

Kumar, S. V., Peters-Lidard, C.D., Mocko, D., Reichle, R., Liu, Y., Arsenault, K.R., Xia, Y., Ek, M., Riggs, G., Livneh, B., Cosh, M., 2014. Assimilation of remotely sensed soil moisture and snow depth retrievals for drought estimation. J. Hydrometeorol. 15, 2446–2469. https://doi.org/10.1175/JHM-D-13-0132.1

Kumar, S. V., Peters-Lidard, C.D., Tian, Y., Houser, P.R., Geiger, J., Olden, S., Lighty, L., Eastman, J.L., Doty, B., Dirmeyer, P., Adams, J., Mitchell, K., Wood, E.F., Sheffield, J., 2006. Land information system: An interoperable framework for high resolution land surface modeling. Environ. Model. Softw. 21, 1402–1415. https://doi.org/10.1016/j.envsoft.2005.07.004

Kumar, S. V., Zaitchik, B.F., Peters-Lidard, C.D., Rodell, M., Reichle, R., Li, B., Jasinski, M., Mocko, D., Getirana, A., De Lannoy, G., Cosh, M.H., Hain, C.R., Anderson, M., Arsenault, K.R., Xia, Y., Ek, M., 2016. Assimilation of Gridded GRACE terrestrial water storage estimates in the North American land data assimilation system. J. Hydrometeorol. 17, 1951–1972. https://doi.org/10.1175/JHM-D-15-0157.1

Li, B., Rodell, M., Kumar, S., Beaudoing, H.K., Getirana, A., Zaitchik, B.F., Goncalves, L.G., Cossetin, C., Bhanja, S., Mukherjee, A., Tian, S., Tangdamrongsub, N., Long, D., Nanteza, J., Lee, J., Policelli, F., Goni, I.B., Daira, D., Bila, M., Lannoy, G., Mocko, D., Steele-Dunne, S.C., Save, H., Bettadpur, S., 2019. Global GRACE Data Assimilation for Groundwater and Drought Monitoring: Advances and Challenges. Water Resour. Res. 1–23. https://doi.org/10.1029/2018wr024618

Lin, P., Pan, M., Beck, H.E., Yang, Y., Yamazaki, D., Frasson, R., David, C.H., Durand, M., Pavelsky, T.M., Allen, G.H., Gleason, C.J., Wood, E.F., 2019. Global Reconstruction of Naturalized River Flows at 2.94 Million Reaches. Water Resour. Res. 55, 6499–6516.

https://doi.org/10.1029/2019WR025287

Luo, X., Li, H.-Y., Ruby Leung, L., Tesfa, T.K., Getirana, A., Papa, F., Hess, L.L., 2017. Modeling surface water dynamics in the Amazon Basin using MOSART-Inundation v1.0: Impacts of geomorphological parameters and river flow representation. Geosci. Model Dev. 10. https://doi.org/10.5194/gmd-10-1233-2017

Martens, B., Miralles, D.G., Lievens, H., van der Schalie, R., de Jeu, R.A.M., Fernández-Prieto, D., Beck, H.E., Dorigo, W.A., Verhoest, N.E.C., 2017. GLEAM v3: satellite-based land evaporation and root-zone soil moisture. Geosci. Model Dev. 10, 1903–1925. https://doi.org/10.5194/gmd-10-1903-2017

McNally, A., Arsenault, K., Kumar, S., Shukla, S., Peterson, P., Wang, S., Funk, C., Peters-Lidard, C.D., Verdin, J.P., 2017. A land data assimilation system for sub-Saharan Africa food and water security applications. Sci. Data 4, 1–19. https://doi.org/10.1038/sdata.2017.12

McNally, A., Verdin, K., Harrison, L., Getirana, A., Jacob, J., Shukla, S., Arsenault, K., Peters-Lidard, C., Verdin, J.P., 2019. Acute Water-Scarcity Monitoring for Africa. Water 11. https://doi.org/10.3390/w11101968

Miguez-Macho, G., Fan, Y., 2012a. The role of groundwater in the Amazon water cycle: 1. Influence on seasonal streamflow, flooding and wetlands. J. Geophys. Res. Atmos. 117, 1–30. https://doi.org/10.1029/2012JD017539

Miguez-Macho, G., Fan, Y., 2012b. The role of groundwater in the Amazon water cycle: 2. Influence on seasonal soil moisture and evapotranspiration. J. Geophys. Res. Atmos. 117. https://doi.org/10.1029/2012JD017540

Miguez-Macho, G., Fan, Y., Weaver, C.P., Walko, R., Robock, A., 2007. Incorporating water table dynamics in climate modeling: 2. Formulation, validation, and soil moisture simulation. J. Geophys. Res. Atmos. 112, 2007. https://doi.org/10.1029/2006JD008112

Monin, A.S., Obukhov, A.M., 1954. Basic laws of turbulent mixing in the surface layer of the atmosphere. Tr. Akad. Nauk. SSSR Geophiz. Inst. 24, 163–187.

Ndehedehe, C., Awange, J., Agutu, N., Kuhn, M., Heck, B., 2016. Understanding changes in terrestrial water storage over West Africa between 2002 and 2014. Adv. Water Resour. 88, 211–230. https://doi.org/10.1016/j.advwatres.2015.12.009

Neal, J., Schumann, G., Bates, P., 2012. A subgrid channel model for simulating river hydraulics and floodplain inundation over large and data sparse areas. Water Resour. Res. 48, 1–16. https://doi.org/10.1029/2012WR012514

Niu, G.-Y., Yang, Z.-L., 2004. Effects of vegetation canopy processes on snow surface energy and mass balances. J. Geophys. Res. Atmos. 109. https://doi.org/10.1029/2004JD004884

Niu, G.-Y., Yang, Z.-L., Dickinson, R.E., Gulden, L.E., Su, H., 2007. Development of a simple groundwater model for use in climate models and evaluation with Gravity Recovery and Climate Experiment data. J. Geophys. Res. 112, D07103.

https://doi.org/10.1029/2006JD007522

Niu, G.Y., Yang, Z.L., Mitchell, K.E., Chen, F., Ek, M.B., Barlage, M., Kumar, A., Manning, K., Niyogi, D., Rosero, E., Tewari, M., Xia, Y., 2011. The community Noah land surface model with multiparameterization options (Noah-MP): 1. Model description and evaluation with local-scale measurements. J. Geophys. Res. Atmos. 116, 1–19. https://doi.org/10.1029/2010JD015139

Noilhan, J., Planton, S., 1989. A Simple Parameterization of Land Surface Processes for Meteorological Models. Mon. Weather Rev. 117, 536–549. https://doi.org/10.1175/1520-0493(1989)117<0536:ASPOLS>2.0.CO;2

O'Loughlin, F.E., Neal, J., Yamazaki, D., Bates, P.D., 2016. ICESat-derived inland water surface spot heights. Water Resour. Res. 52, 3276–3284. https://doi.org/10.1002/2015WR018237

Paiva, R.C.D., Collischonn, W., Bonnet, M.-P., De Gonçalves, L.G.G., Calmant, S., Getirana, A., Santos Da Silva, J., 2013a. Assimilating in situ and radar altimetry data into a large-scale hydrologic-hydrodynamic model for streamflow forecast in the Amazon. Hydrol. Earth Syst. Sci. 17. https://doi.org/10.5194/hess-17-2929-2013

Paiva, R.C.D., Collischonn, W., Buarque, D.C., 2013b. Validation of a full hydrodynamic model for large-scale hydrologic modelling in the Amazon. Hydrol. Process. 27, 333–346. https://doi.org/10.1002/hyp.8425

Poméon, T., Jackisch, D., Diekkrüger, B., 2017. Evaluating the performance of remotely sensed and reanalysed precipitation data over West Africa using HBV light. J. Hydrol. 547, 222–235. https://doi.org/10.1016/j.jhydrol.2017.01.055

Reichle, R.H., Liu, Q., Koster, R.D., Draper, C.S., Mahanama, S.P.P., Partyka, G.S., 2017. Land Surface Precipitation in MERRA-2. J. Clim. 30, 1643–1664. https://doi.org/10.1175/JCLI-D-16-0570.1

Rodell, M., Famiglietti, J.S., Wiese, D.N., Reager, J.T., Beaudoing, H.K., Landerer, F.W., Lo, M.H., 2018. Emerging trends in global freshwater availability. Nature 557, 651–659. https://doi.org/10.1038/s41586-018-0123-1

Rodell, M., Houser, P.R., Jambor, U., Gottschalck, J., Mitchell, K., Meng, C.J., Arsenault, K., Cosgrove, B., Radakovich, J., Bosilovich, M., Entin, J.K., Walker, J.P., Lohmann, D., Toll, D., 2004. The Global Land Data Assimilation System. Bull. Am. Meteorol. Soc. 85, 381–394. https://doi.org/10.1175/BAMS-85-3-381

Ronneberger, O., Fischer, P., Brox, T., 2015. U-Net: Convolutional Networks for Biomedical Image Segmentation, in: Navab, N., Hornegger, J., Wells, W.M., Frangi, A.F. (Eds.), Medical Image Computing and Computer-Assisted Intervention -- MICCAI 2015. Springer International Publishing, Cham, pp. 234–241.

Santos da Silva, J., Calmant, S., Seyler, F., Rotunno Filho, O.C., Cochonneau, G., Mansur, W.J., 2010. Water levels in the Amazon basin derived from the ERS 2 and ENVISAT radar

altimetry missions. Remote Sens. Environ. 114, 2160–2181. https://doi.org/10.1016/j.rse.2010.04.020

Schrapffer, A., Sörensson, A., Polcher, J., Fita, L., 2020. Benefits of representing floodplains in a Land Surface Model: Pantanal simulated with ORCHIDEE CMIP6 version. Clim. Dyn. 55, 1303–1323. https://doi.org/10.1007/s00382-020-05324-0

Shukla, S., Arsenault, K., Hazra, A., Peters-Lidard, C., Koster, R., Davenport, F., Magadzire, T., Funk, C., Kumar, S., McNally, A., Getirana, A., Husak, G., Zaitchik, B., Verdin, J., Nsadisa, F.D., Becker-Reshef, I., 2019. Improving early warning of drought-driven food insecurity in Southern Africa using operational hydrological monitoring and forecasting products. Nat. Hazards Earth Syst. Sci. Discuss. 1–29. https://doi.org/10.5194/nhess-2019-267

Tourian, M.J., Schwatke, C., Sneeuw, N., 2017. River discharge estimation at daily resolution from satellite altimetry over an entire river basin. J. Hydrol. 546, 230–247. https://doi.org/10.1016/j.jhydrol.2017.01.009

Tourian, M.J., Tarpanelli, A., Elmi, O., Qin, T., Brocca, L., Moramarco, T., Sneeuw, N., 2016. Spatiotemporal densification of river water level time series by multimission satellite altimetry. Water Resour. Res. 52, 1140–1159. https://doi.org/10.1002/2015WR017654

Urban, T.J., Schutz, B.E., Neuenschwander, A.L., 2008. A Survey of ICESat Coastal Altimetry Applications: Continental Coast, Open Ocean Island, and Inland River. Terr. Atmos. Ocean. Sci. 19, 1. https://doi.org/10.3319/TAO.2008.19.1-2.1(SA)

Walko, R.L., Band, L.E., Baron, J., Kittel, T.G.F., Lammers, R., Lee, T.J., Ojima, D., Pielke, R.A., Taylor, C., Tague, C., Tremback, C.J., Vidale, P.L., 2000. Coupled Atmosphere–Biophysics–Hydrology Models for Environmental Modeling. J. Appl. Meteorol. 39, 931–944. https://doi.org/10.1175/1520-0450(2000)039<0931:CABHMF>2.0.CO;2

Whyte, A., Ferentinos, K.P., Petropoulos, G.P., 2018. A new synergistic approach for monitoring wetlands using Sentinels -1 and 2 data with object-based machine learning algorithms. Environ. Model. Softw. 104, 40–54. https://doi.org/10.1016/j.envsoft.2018.01.023

Xia, Y., Mitchell, K., Ek, M., Cosgrove, B., Sheffield, J., Luo, L., Alonge, C., Wei, H., Meng, J., Livneh, B., Duan, Q., Lohmann, D., 2012. Continental-scale water and energy flux analysis and validation for North American Land Data Assimilation System project phase 2 (NLDAS-2): 2. Validation of model-simulated streamflow. J. Geophys. Res. Atmos. 117, 1–23. https://doi.org/10.1029/2011JD016051

Yamazaki, D., Ikeshima, D., Sosa, J., Bates, P.D., Allen, G.H., Pavelsky, T.M., 2019. MERIT Hydro: A High-Resolution Global Hydrography Map Based on Latest Topography Dataset. Water Resour. Res. https://doi.org/10.1029/2019WR024873

Yamazaki, D., Ikeshima, D., Tawatari, R., Yamaguchi, T., O'Loughlin, F., Neal, J.C., Sampson, C.C., Kanae, S., Bates, P.D., 2017. A high-accuracy map of global terrain elevations. Geophys. Res. Lett. 44, 5844–5853. https://doi.org/10.1002/2017GL072874

Yamazaki, D., Sato, T., Kanae, S., Hirabayashi, Y., Bates, P.D., 2014. Regional flood dynamics in a bifurcating mega delta simulated in a global river model. Geophys. Res. Lett. 41, 3127–3135. https://doi.org/10.1002/2014GL059744

Yang, Z.-L., Niu, G.-Y., Mitchell, K.E., Chen, F., Ek, M.B., Barlage, M., Longuevergne, L., Manning, K., Niyogi, D., Tewari, M., Xia, Y., 2011. The community Noah land surface model with multiparameterization options (Noah-MP): 2. Evaluation over global river basins. J. Geophys. Res. Atmos. 116. https://doi.org/10.1029/2010JD015140